Proceedings of the
Second International Pump Symposium

Sponsored by the
Turbomachinery Laboratories
Department of Mechanical Engineering
Texas A&M University
College Station, Texas

Dr. Dara Childs, P.E., Director
Dr. Jean C. Bailey, Editor
with assistance from
The Advisory Committee
and
The Staff of the Turbomachinery Laboratories

April 1985

FORCES ON CENTRIFUGAL PUMP IMPELLERS

by

Belgacem Jery
Graduate Student
Christopher E. Brennen
Professor
Thomas K. Caughey
Professor
and
Allan Acosta
Professor
Division of Engineering and Applied Science
California Institute of Technology
Pasadena, California

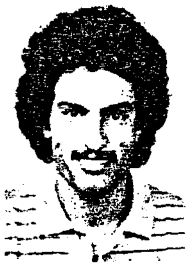

Belgacem Jery is a Graduate Student at the California Institute of Technology in Pasadena, California. Mr. Jery holds an Engineer Diploma from ENSAM in Paris, France. His M.S. in Mechanical Engineering degree is from Caltech, Pasadena, California. Mr. Jery has conducted graduate research on rotor instability in high performance turbomachines as part of his Ph.D. work. He has published several papers on this subject. He is a member of ASME and Societe des Ingenieurs ENSAM.

Christopher E. Brennen is a Professor of Mechanical Engineering in the Division of Engineering and Applied Science, at the California Institute of Technology in Pasadena, California.

He holds B.A., M.A. and Ph.D. degrees in Engineering Science from Oxford University. Dr. Brennen was a Fulbright Scholar from 1969 to 1971. He has been honored by ASME, is a consultant and has many technical publications.

Thomas K. Caughey is a Professor of Applied Mechanics at the California Institute of Technology in Pasadena, California.

He received B.Sc. and M.E. degrees from Glasgow University in 1948, an M.M.E. degree from Cornell University in 1952 and a Ph.D. degree in Engineering Science from California Institute of Technology in 1954.

Dr. Caughey's fields of interest are Applied Mathematics, Dynamics, Vibrations, Acoustics, Stability, Non-linear Systems, Stochastic Processes, Chaos and Control Theory.

Allan J. Acosta, Professor of Mechanical Engineering at the California Institute of Technology since 1954, is currently involved in the study of internal flows in hydraulic machinery and fluid-structure interactions in these machines. He has also studied cavitation effects in hydraulic machinery and cavitation inception as it occurs in applications of naval hydrodynamics.

Prior to joining Caltech, he worked on model pumps for the Grand Coulee Irrigation Project. In 1954, he joined Caltech's Hydrodynamics Research Laboratory and worked on problems in centrifugal pump impellers, axial flow pumps and inducers and cavitating hydrofoils.

A Fellow of ASME, Dr. Acosta is a two-time recipient of the Knapp Award, and received the Moody Award, the 1975 ASME Melville Medal, and the Henry R. Worthington award in 1982. He has been chairman of the Ocean Engineering Division (1967) and the Fluids Engineering Division (1980).

A registered professional engineer in the State of California, he is also a member of the International Association of Hydraulic Research, the American Association for the Advancement of Science, the Society of Naval Architects and Marine Engineers and Sigma Xi.

ABSTRACT

Forces are exerted on a centrifugal pump impeller, due to the asymmetry of the flow caused by the volute or diffuser, and to the motion of the center of the impeller whenever the shaft whirls. Recent work in the measurement of these forces, as a function of the whirl speed to shaft speed ratio, and the influence of the volute, is reviewed. These forces may be decomposed into a steady force, a static stiffness matrix, a damping matrix and an inertia matrix. It is shown that for centrifugal pumps of the moderate specific speed typical of boiler feed stages, there is a region of potential shaft vibration excitation from the hydrodynamic forces if the operating speed is well above the first flexural critical speed.

INTRODUCTION

The need for more powerful, more efficient and more reliable turbomachines has grown substantially in the past decade. As a result, a great deal of effort is being devoted to solving increasingly complex design and manufacturing problems. One such problem is a self-excited rotor vibration phenomenon widely known now as rotor whirl. The research work described herein is an experimental investigation of rotor whirl related instabilities in centrifugal flow pumps. This investigation is part of an on-going program that started in 1977 at the California Institute of Technology, under the sponsorship of NASA, in conjunction with the development of the Space Shuttle Main Engine (SSME). A recent article by Ehric and Childs [1] provides excellent background information on the subject of rotor whirl in general. As far as the present research is concerned, detailed descriptions of the test program, the experimental setup and the preliminary findings of the investigation exist elsewhere in the literature [2,3,4,5,6,7]. References [4] and [7] are especially recommended. Contributions from other sources are also noted in the literature [8,9,10,11,12,13,14]. More recent experimental test results are reported herein. A discussion is provided of the measured hydrodynamic stiffness, damping and inertia coefficients and their relation to the various impeller and volute or diffuser ~~geometries and~~ to the wide range of flow conditions. Finally, an example which illustrates the practical use of these rotordynamic coefficients is provided.

EXPERIMENTAL OBJECTIVE

When introducing a new turbomachine design, engineers generally agree that model testing is the only sure way to predict the dynamic behavior, especially for operation off-design. If done for every new product, this can prove to be very costly. However, the lack of theoretical data leaves very little choice to the designer. Empiricism, intuition, and past practical experience are usually brought into play. Another alternative is to conduct a limited, but very carefully selected, set of experiments, in which key parameters are varied and tested in a systematic fashion. Results of such tests can be extended to a much larger class of machines and operating conditions, by the use of simple scaling (similarity) laws. This was the approach chosen in the current experimental work. The objective herein is to provide designers of centrifugal flow pumps with a deeper understanding of the role of hydrodynamic impeller-volute diffuser interactions in the excitation or damping of rotor whirl. From a rotordynamics point of view, this means providing impeller-volute diffuser hydrodynamic stiffness, damping and inertia coefficients to be used in determining the critical speeds and the Onset Speed of Instability (OSI).

EXPERIMENTAL PROCEDURE

To measure these rotordynamic coefficients, it was decided to perform what amounts to a set of *forced vibration* tests. The rotor of a centrifugal pump is forced into a whirling motion in which the impeller center is made to follow a circular orbit, at a constant angular rate Ω, while the impeller axis remains parallel to the pump centerline. This takes place in addition to and independently of the normal impeller rotation at the constant angular rate ω. The whirl orbit center coincides with the volute or diffuser geometric center 0 (Figure 1). The orbit radius ϵ is constant and its value of 1.3 mm was carefully chosen: too large an ϵ would void the assumption of small perturbations; too small an ϵ would result in forces not large enough to be measured accurately. The word "forces" here refers to the components of the generalized hydrodynamic force vector $\{F\}$ acting on the impeller as it undergoes simultaneous whirl and rotation.

All six components of $\{F\}$ are sensed by a rotating dynamometer, strategically placed between the impeller and the drive shaft to avoid any drive system noise and unwanted forces. By design, both the shaft and the dynamometer could be considered infinitely rigid for the purpose of these measurements. Since whirl is usually associated with the lateral deflection of the rotor, only two of vector $\{F\}$ components will be discussed, namely, the two lateral hydrodynamic forces F_x and F_y acting at the impeller center, in a plane perpendicular to the machine axis of rotation. Referring to Figure 1, these forces can be written in the form:

$$\begin{Bmatrix} F_x \\ F_y \end{Bmatrix} = \begin{Bmatrix} F_{ox} \\ F_{oy} \end{Bmatrix} + [A] \begin{Bmatrix} x \\ y \end{Bmatrix} \qquad (1)$$

where x and y represent the coordinates of the impeller center measured from the center of the volute 0. In both this equation and all the equations and results which follow, dimensionless quantities are used. The linear form of equation (1) assumes small offsets x and y as allowed by the choice of ϵ. At the present time little is known of the possible non-linear effects.

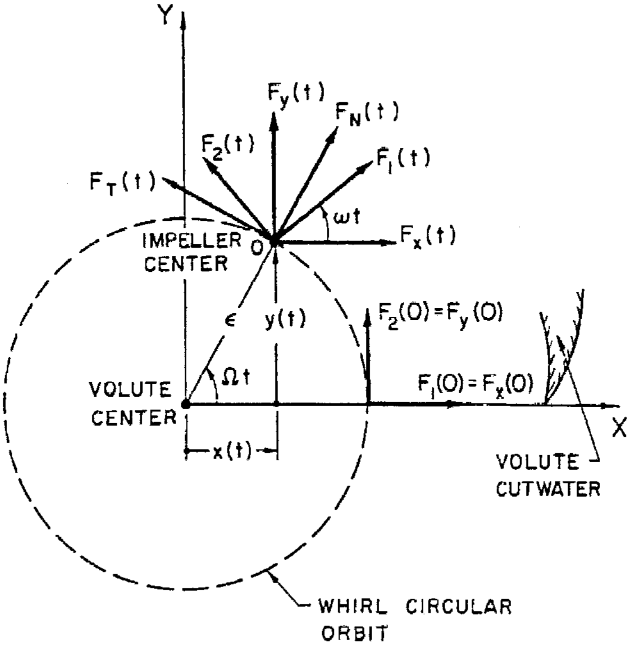

Figure 1. Schematic Diagram Representing the Lateral Forces in the Rotating Dynamometer Frame (F_1,F_2), in the Stationary Volute Frame (F_x,F_y) and in the Local Polar Coordinate Frame (F_N,F_T).

When x and y are *fixed* in time, F_x and F_y represent the *steady* lateral forces, and can be viewed as the sum of two forces: a fixed force (F_{ox} and F_{oy} would be only forces present, should the impeller center coincide with the volute center, i.e., $x=y=0$) and a quantity proportional to the displacement, which represents a static fluid "stiffness" effect. These two quantities have been the subject of previous reports [3,4,5,6]. Herein, the analysis and experiments for the case of non-zero whirl velocity, in which x and y are harmonic functions of time, ($x=x(t)=\epsilon \cos \Omega t/r_2$, $y=y(t)=\epsilon \sin \Omega t/r_2$), will be discussed. Damping and inertia effects are associated with the harmonic velocities and accelerations $\dot{x}$, $\dot{y}$, $\ddot{x}$, $\ddot{y}$ of the impeller center. In this case, equation (1) can be generalized to the form:

$$\begin{Bmatrix} F_x(t) \\ F_y(t) \end{Bmatrix} = \begin{Bmatrix} F_{ox} \\ F_{oy} \end{Bmatrix} + [A(\Omega/\omega)] \begin{bmatrix} \epsilon/r_2 \cos \Omega t \\ \epsilon/r_2 \cos \Omega t \end{bmatrix} \tag{2}$$

The second quantity on the right hand side of Equation (2) represents the *unsteady* forces resulting from the combined motions of the impeller. Notice that what was a pure force matrix [A] in equation (1) is now a "generalized" force matrix $[A(\Omega/\omega)]$. Indeed, the primary purpose of the unsteady measurements was to establish the functional form of this matrix when Ω/ω is varied. However, the matrices required for input into most rotordynamic analyses are the stiffness [K], damping [C], and inertial [M], matrices defined by the dimensionless matrix equation:

$$\begin{Bmatrix} F_x \\ F_y \end{Bmatrix} = \begin{Bmatrix} F_{ox} \\ F_{oy} \end{Bmatrix} - [M] \begin{Bmatrix} \ddot{x} \\ \ddot{y} \end{Bmatrix} - [C] \begin{Bmatrix} \dot{x} \\ \dot{y} \end{Bmatrix} - [K] \begin{Bmatrix} x \\ y \end{Bmatrix} \tag{3}$$

It follows, by comparing the definitions (2) and (3), that

$$A_{xx} = M_{xx} \frac{\Omega^2}{\omega^2} - C_{xy} \frac{\Omega}{\omega} - K_{xx}$$

$$A_{xy} = M_{xy} \frac{\Omega^2}{\omega^2} + C_{xx} \frac{\Omega}{\omega} - K_{xy}$$

$$A_{yx} = M_{yx} \frac{\Omega^2}{\omega^2} - C_{yx} \frac{\Omega}{\omega} - K_{yx}$$

$$A_{yy} = M_{yy} \frac{\Omega^2}{\omega^2} + C_{yx} \frac{\Omega}{\omega} - K_{yy} \tag{4}$$

The identities (4) suggested the following data acquisition and reduction procedure: for each impeller-volute/diffuser combination, pump speed ω and flow coefficient ϕ, a set of force measurements was taken varying *only* the whirl velocity Ω. These measurements were processed, resulting in a set of generalized stiffness matrices, one for each value of Ω/ω.

At this point it should be observed that Equation (3) makes the a priori assumption that the elements A_{ij} of the matrix $[A(\Omega/\omega)]$ vary quadratically with Ω/ω. In the absence of any fundamental reason supporting this assumption, it was decided to report the measured values of these elements in the form of curves of A_{ij} versus Ω/ω. The elements of [M], [C], and [K] are estimated from these curves, using least squares quadratic fits.

TEST MATRIX

Treatment of Tare Forces

Three primary sources of tare forces were identified:

(a) gravitational and pure mass inertial loads on the rotor
(b) the buoyancy force on the submerged impeller and dynamometer
c) parasitic hydrodynamic forces on the external surfaces of the submerged dynamometer.

Forces (a) were removed by subtracting the forces measured in a "dry" run, where the impeller was operated in *air*, from the forces measured in a "wet" run, where the same impeller was operated in *water* at the same speeds Ω and ω. Thus, each data point was determined from the results of two separate tests.

Provision was also made in the software to subtract out force (b) which is simply equal to the weight of the dry rotor, minus that of the submerged rotor (as measured by the dynamometer when the rotor was still). A recent modification of the hardware (enlargement of the gap surrounding the dynamometer shield) made it possible to neglect forces (c). Indeed, these forces now represent less than three percent of the impeller forces. Before this modification, parasitic forces were as high as 10 percent of the impeller forces. It was then necessary to subtract these parasitic forces. This required performing two additional runs for each eventual data point: a wet run without impeller and a dry run without impeller.

Subsequent to this and other minor hardware modifications, a complete recalibration of the dynamometer took place and all the previous measurements were repeated. The present data include results from these reruns for the sake of completeness.

Test Matrix

To date, over 75 sets of measurements have been made. In each of these sets Ω was varied while ω and ϕ were held constant. This brings the total of individual test runs to over 900. Altogether three impellers (one five-bladed (Impeller X), one six-bladed (Impeller Y) and a solid dummy (Impeller S)) and seven volute/diffuser volutes (Volutes A and D, Diffuser Volutes E, F, G and H; and N, referring to the absence of any volute) were tested under various combinations of pump speeds (500, 1000, 1500, and 2000 rpm) and flow coefficients ($\phi = 0$ (shutoff), 0.03, 0.06, 0.092 (design ϕ for Impeller X), 0.110, and $\phi = \phi_{max}$ (throttle full open).

Appendix A gives a summary of the characteristics of the various volutes/diffusers and the different impellers. All tests were conducted using the same impeller face seal clearance of 0.13 mm.

As a precautionary measure to limit the inertial loads and mechanical vibrations on the rotor assembly, the maximum whirl speed was kept at 1200 rpm. The following ranges for the value of Ω/ω resulted:

(a) $-0.6 \leq \Omega/\omega \leq 0.6$ for 2000 rpm pump speed
(b) $-0.7 \leq \Omega/\omega \leq 0.8$ for 1500 rpm pump speed
(c) $-0.9 \leq \Omega/\omega \leq 1.1$ for 1000 rpm pump speed
(d) $-2.0 \leq \Omega/\omega \leq 2.0$ for 500 rpm pump speed

The negative sign in the inequalities refers to the negative whirl directions. Thus, both subsynchronous and supersynchronous whirl motions were explored in both directions.

TEST RESULTS

Data such as the average lateral forces (F_{ox}, F_{oy}), the steady and unsteady thrust, torque and bending moments and the hydraulic performance curves ($\psi(\phi)$) will be presented in later reports. The measured hydrodynamic force matrices $[A(\Omega/\omega)]$ results are presented herein. Data on these matrices can be presented in any one of three formats:

(a) graphs of the individual elements of $[A(\Omega/\omega)]$ as a function of Ω/ω.

(b) graphs of the average normal and tangential forces (F_N and F_T) given by:

$$F_N = \tfrac{1}{2}(A_{xx} + A_{yy})$$

$$F_T = \tfrac{1}{2}(-A_{xy} + A_{yx})$$

(c) tables of stiffness, damping and inertia coefficients obtained from second order least squares fits as defined in Equations (3) and (4).

The first format has the advantage of reporting the data in their raw and complete form, but is not always convenient to work with. Typical results from a sample case are shown in Figure 2, using this format. The measurements were made using the combination Volute A/Impeller X, which was tested more extensively than any other combination. Volute A was designed to match Impeller X at its shock-free entry condition with a flow coefficient $\phi = 0.092$. The elements of $[A(\Omega/\omega)]$ obtained when this combination was tested at the design flow coefficient, with the pump running at 1000 rpm and the impeller face seal clearance set at 0.13 mm, are shown in Figure 2, plotted against I/J (or Ω/ω, equivalently, see NOMENCLATURE).

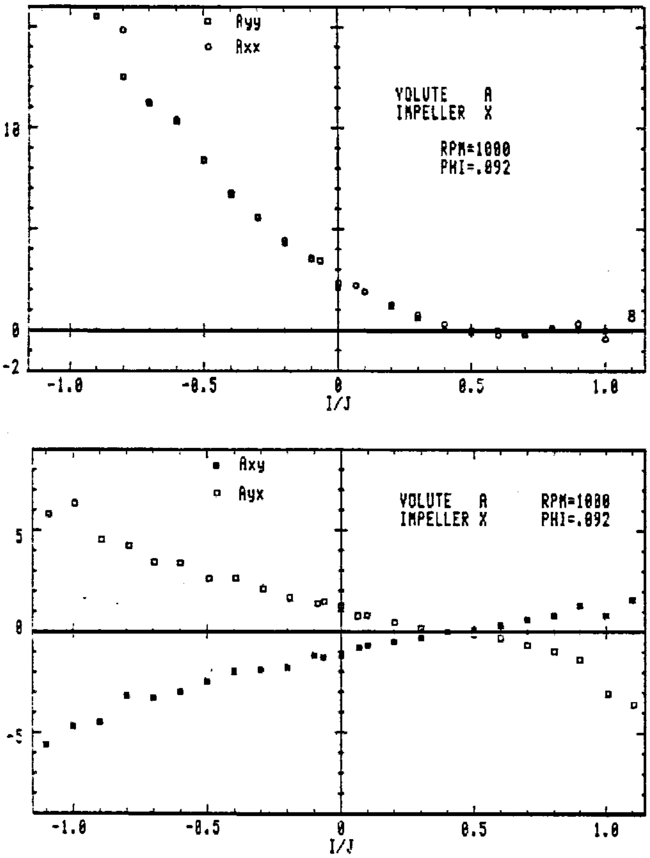

Figure 2. The Elements of the Hydrodynamic Force Matrix, [A], as a Function of Ω/ω, for the Volute A Impeller X Combination at 1000 RPM and the Impeller X Design Flow Coefficient $\phi = 0.092$.

Examination of these graph shows that matrix $[A(\Omega/\omega)]$ has almost equal diagonal terms and off-diagonal terms which are almost equal, but of opposite sign. This skew-symmetric form of the hydrodynamic matrix is remarkable since there is no known fundamental reason why this should be the case. This form has often been *assumed* but this is the first confirmation of which the authors are aware. Also, this form of the matrix makes the (F_N, F_T) format very convenient. The values of F_N and F_T corresponding to Figure 2 are shown in Figure 3. The graphs in Figure 3 carry the same information as those in Figure 2, but in a much more synoptic form. From here on graphic representation of all test results will be confined to the (F_N, F_T) format.

Several general features of these results should be emphasized. Considering F_N, note that the hydrodynamic force was almost always in the radially outward direction. At zero whirl frequency, it had a positive value which is in close agreement with the results of Chamieh, et al. [3,4,5]. This corresponds to a negative stiffness at zero whirl speed. The sign of the tangential force, F_T, is such as to produce a rotordynamically stabilizing effect at negative whirl speeds and for the larger positive whirl speeds. However, it is important to note that there was a region of positive whirl speeds between zero and $\Omega/\omega = 0.25 \rightarrow 0.5$ in which the tangential force is destabilizing rotordynamically.

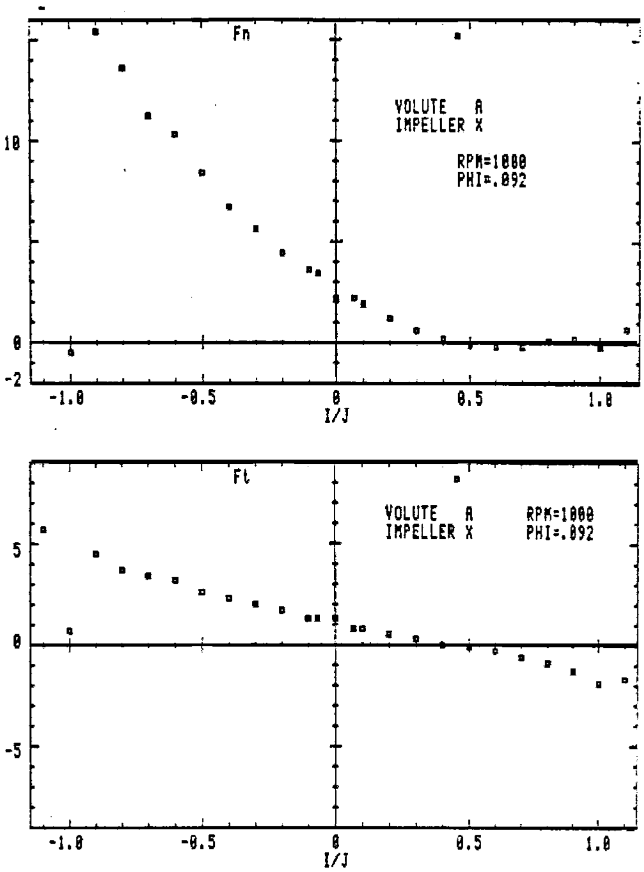

Figure 3. The Dimensionless Average Normal and Tangential Forces, F_N, F_T, Corresponding to Figure 2.

Effect of Pump Speed

Conventional scaling of forces in pumps imply that data obtained when varying only the pump speed should be identical when plotted in the appropriate dimensionless form. This is indeed the case for both F_N and F_T (for both design and off design flow conditions), when the present non-dimensionalization is used, as is demonstrated in Figures 4 and 5.

Effect of Flow Coefficient

The dependence of the hydrodynamic forces on the flow coefficient is illustrated in Figure 6 for the 1000 rpm pump speed. The data shown were obtained with a diffuser volute, diffuser Volute E and Impeller X. Both F_N and F_T show a clear dependence on the value of ϕ throughout the whirl speed range. Of particular interest, however, is the shift in the value Ω/ω at which F_T changes sign. At shutoff ($\phi = 0$), this value was negative ($\Omega/\omega = -0.2$), indicating a whirl stabilizing tangential force for *all* speed ratios. As ϕ is increased to 0.060, the sign change occurred in the positive whirl region and at a much higher speed ratio ($\Omega/\omega = +0.5$). Accordingly, F_T had a destabilizing effect in the positive subsynchronous whirl region between $\Omega/\omega = 0$ and $\Omega/\omega = 0.5$. However, as ϕ was increased even further, an interesting reduction in the critical value of Ω/ω was evident—at and above design ($\phi = 0.092$ and $\phi = \phi_{max}$) the destablizing effect was confined to the region $0 \leq \Omega/\omega \leq 0.3$.

Further study of these curves revealed interesting information concerning the curvature of the graph of the average tangential force. At shutoff, this curvature undergoes several changes (from positive, to negative, to positive again). As the flow coefficient is increased, these changes become less pro-

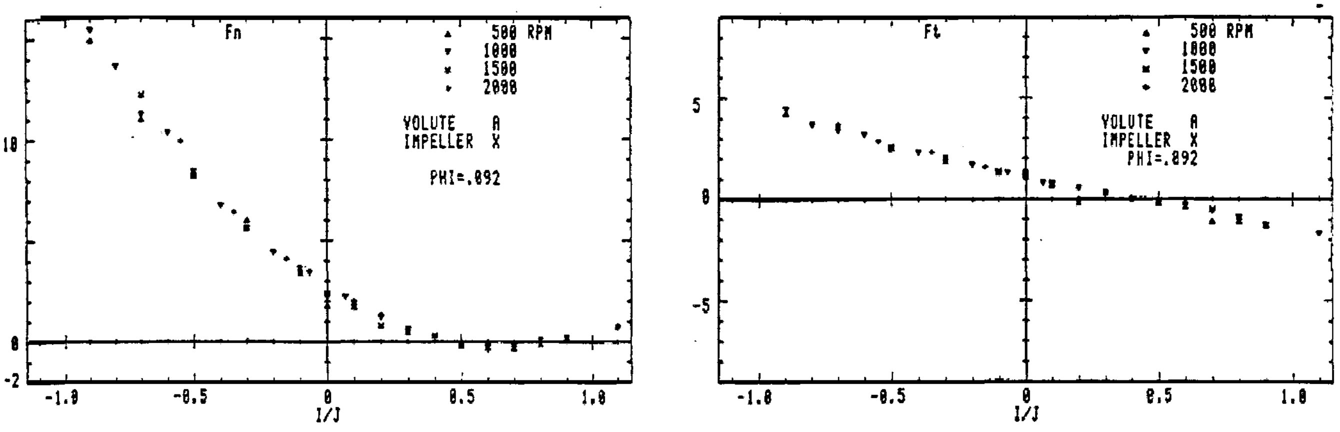

Figure 4. The Average Normal and Tangential Forces for Volute A/Impeller X at the Impeller X Design Flow Coefficient $\phi = 0.092$ and Four Different Pump Speeds: 500, 1000, 1500 and 2000 RPM.

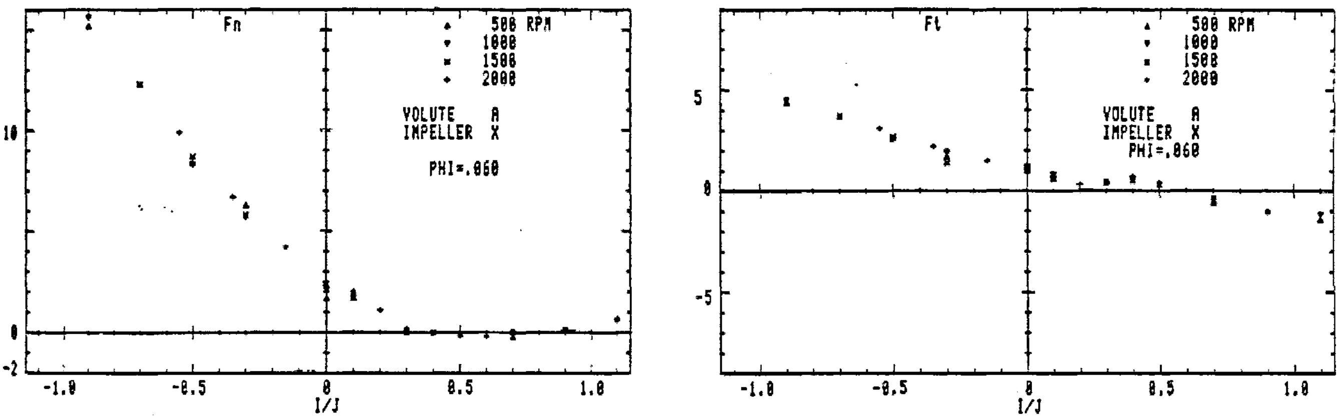

Figure 5. The Average Normal and Tangential Forces for Volute A/Impeller X at Below Design Flow Coefficient ($\phi = 0.060$) and Four Different Pump Speeds: 500, 1000, 1500 and 2000 RPM.

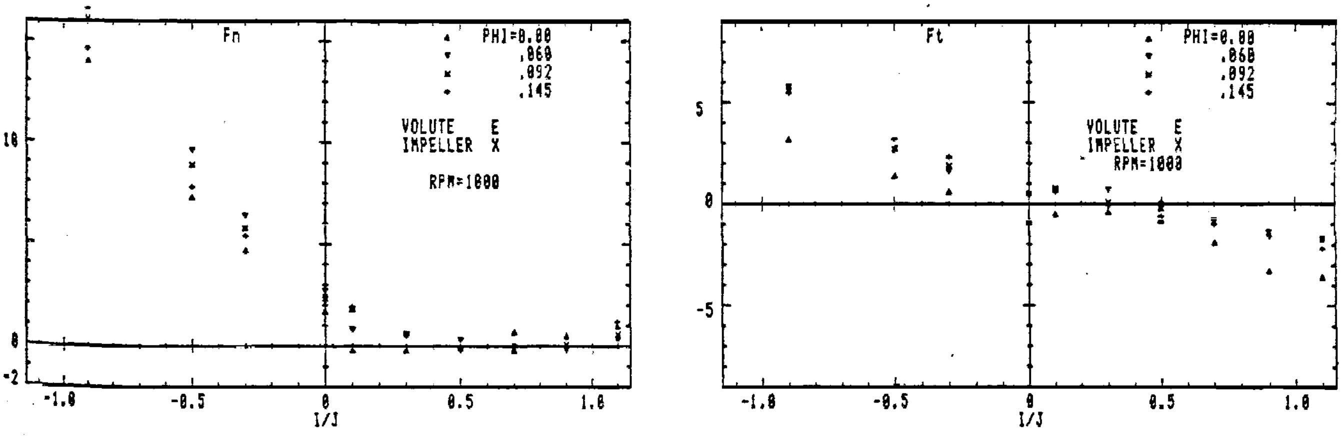

Figure 6. The Average Normal and Tangential Forces for Volute E/Impeller X at 1000 RPM Pump Speed and Four Different Flow Coefficients: $\phi = 0$, 0.060, 0.092 and 0.145.

nounced, ending in a uniform positive curvature at maximum flow.

To better illustrate the evolution of the curvature with increasing flow coefficients, two additional sets of measurements were taken at selected intermediate values of ϕ,($\phi = 0.030$ and 0.110). The corresponding F_T curves are presented separately in Figure 7 (for clarity). Particularly noteworthy is the fact that, at $\phi = 0.030$, F_T changed sign twice in the positive whirl speed region: first, sloping upward at around $\Omega/\omega = 0.05$, then downward at around $\Omega/\omega = 0.2$.

Effects of Volute Geometry

Effects of the volute geometry are presented in Figures 8 and 9. In Figure 8, comparison is made between the results obtained when Impeller X was operated inside Volute A, and when the same impeller was operated inside the pump casing (without any volute—crudely approximating the case where the impeller is whirling in an infinite media). One clearly observes a much stronger interaction due to the presence of a volute, resulting in a much wider destablizing region $(0 \leq \Omega/\omega \leq 0.6$

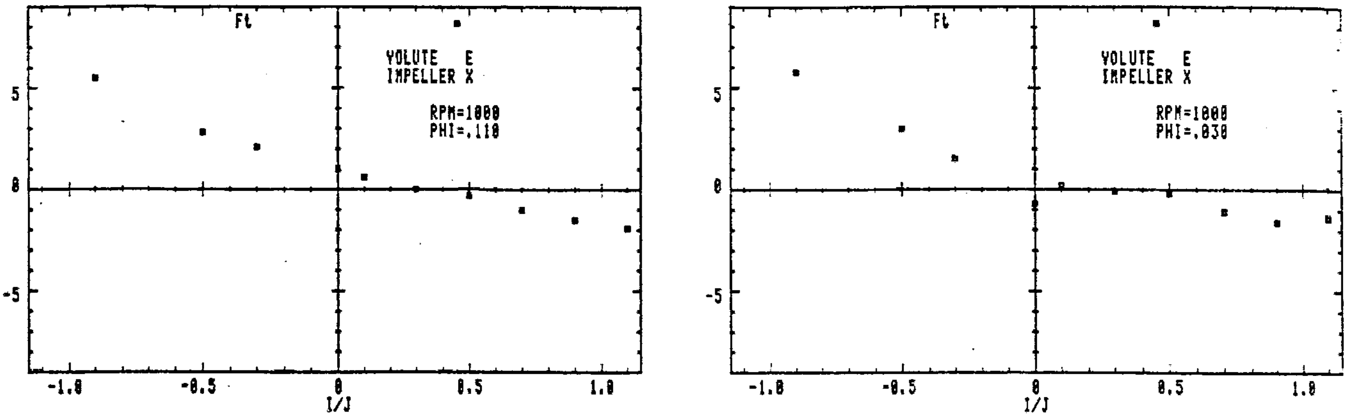

Figure 7. The Average Tangential Force for Volute E/Impeller X at 1000 RPM Pump Speed and Two Flow Coefficients: $\phi = 0.030$ and $\phi = 0.110$.

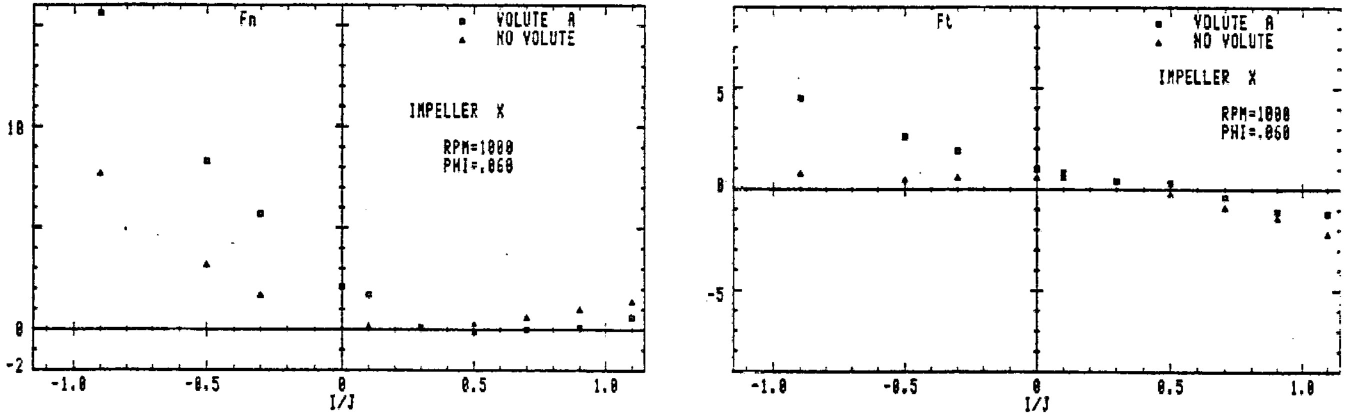

Figure 8. The Average Normal and Tangential Forces for Impeller X with and without Volute A. The pump speed is 1000 rpm and the flow coefficient is $\phi = 0.060$.

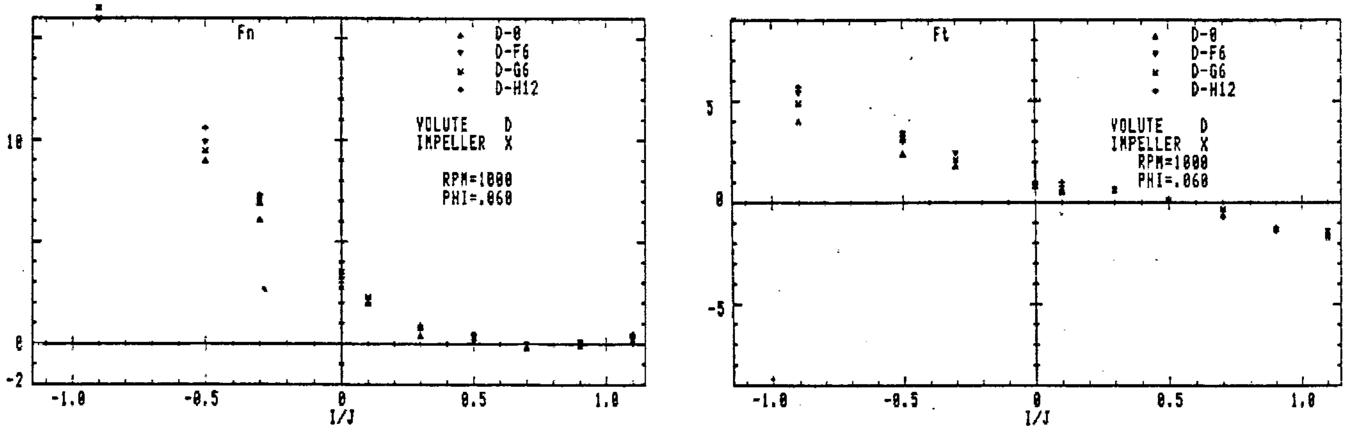

Figure 9. The Average Normal and Tangential Force for Impeller X and Four Different Diffuser Volutes (see APPENDIX A). The pump speed is 1000 rpm and the flow coefficient is $\phi = 0.060$.

compared to $0 \leq \Omega/\omega \leq 0.4$ with no volute). On the other hand, the presence of diffuser guide vanes (or their number or orientation) appeared to have little effect on F_N and F_T (Figure 9). Data in this figure were obtained with the same diffuser volute. Diffuser Volute D was first tested with no vanes (D-0), then with two different sets of six vanes at two different angles (D-F6 and D-G6), and finally with a set of 12 vanes (D-H12). Detailed information on the impellers and volutes utilized in this testing is presented in APPENDIX A.

Effect of Impeller Geometry

Although Impeller X and Impeller Y have a different number of vanes (five for X and six for Y), their hydraulic characteristics are quite similar. It is therefore not a great surprise that the forces measured on these two impellers had very much the same magnitude and phase. This is demonstrated in Figure 10, where the pump speed was 1000 rpm and the flow coefficient was kept at the Impeller X design value (0.092).

Presently, skin friction and leakage flow through the impeller face seals are being investigated. Preliminary measurement results are presented in Figure 11. The comparison here is between the forces measured on Impeller X and those measured on a consolidated dummy (Impeller S, duplicating the exterior geometry of Impeller X). Both measurements were made at shutoff ($\phi = 0$), with the pump running at 1000 rpm. A noticeable difference can be observed in both F_N and F_T.

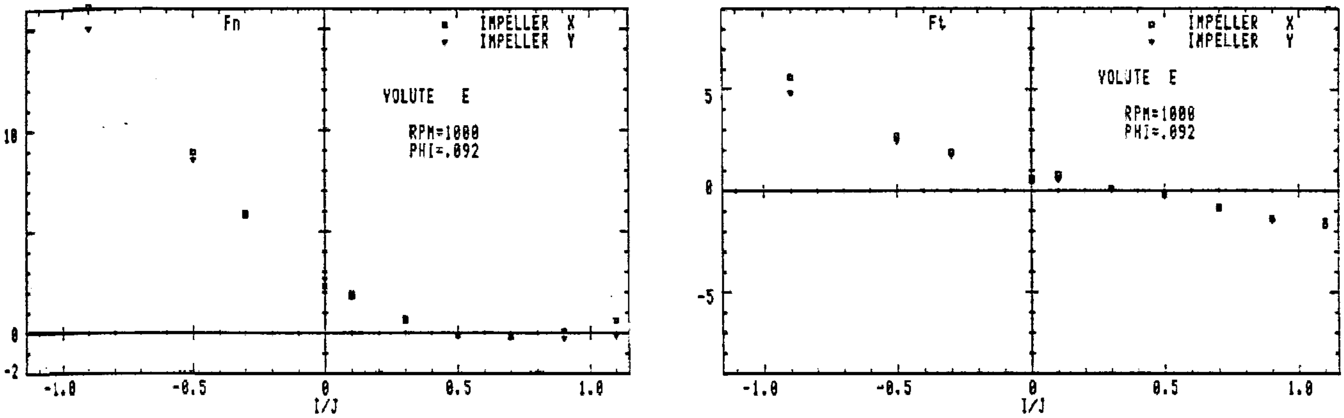

Figure 10. The Average Normal and Tangential Forces for Diffuser Volute E and Two Different Impellers (Impeller X and Impeller Y). The pump speed is 1000 rpm and the flow coefficient is $\phi = 0.092$ = Impeller X design flow coefficient.

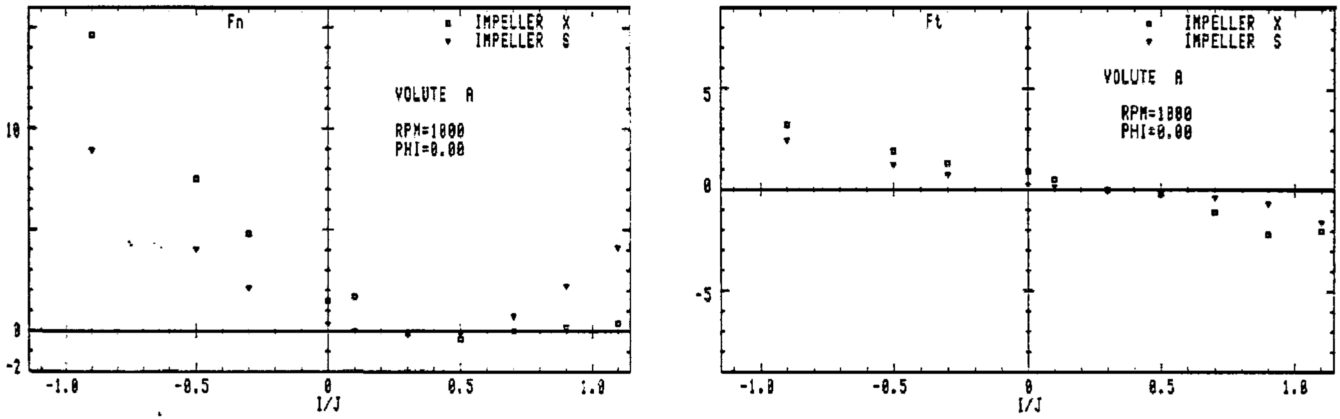

Figure 11. The Average Normal and Tangential Forces for Volute A and Two Different Impellers (Impeller X and Impeller S). The pump was run at shutoff at 1000 rpm.

Table 1. Impeller Rotordynamics Coefficients

VOLTE SPEED	IMPEL. PHI	Kxx Kyx	Kxy Kyy	Cxx Cyx	Cxy Cyy	Mxx Myx	Mxy Myy
A 500	X 0.092	-2.375 -1.094	1.100 -2.640	2.934 -8.141	7.685 3.341	6.906 0.358	-0.697 6.127
A 1000	X 0.092	-2.681 -1.220	1.011 -2.532	2.894 -8.477	8.568 3.660	6.186 0.294	-0.774 6.302
A 1500	X 0.092	-2.541 -1.078	0.901 -2.390	2.877 -8.704	8.709 3.116	6.979 0.628	-1.114 6.761
A 2000	X 0.092	-2.687 -1.239	1.062 -2.596	2.887 -9.006	9.108 3.009	6.928 0.640	-0.693 7.110
E 1000	X 0.000	-1.893 -0.133	0.145 -1.387	3.449 -7.279	7.035 3.350	6.183 -0.923	0.433 7.483
E 1000	X 0.060	-2.805 -0.992	1.043 -2.710	3.662 -9.421	9.647 3.011	6.581 1.021	-0.998 7.259
E 1000	X 0.092	-2.699 -0.967	1.104 -2.572	3.728 -8.846	9.071 3.871	6.222 0.926	-0.880 6.978
E 1000	X 0.145	-2.546 -1.157	1.169 -2.343	4.101 -7.770	8.090 4.127	5.624 0.437	-0.661 6.774
N 1000	X 0.060	-0.646 -0.739	0.611 -0.462	1.135 -3.575	3.627 1.337	4.249 -2.098	1.265 4.507
D 1000	X 0.060	-2.996 -1.165	1.069 -2.725	2.626 -9.193	9.290 2.992	6.254 -0.102	-0.401 6.603
F 1000	X 0.060	-3.454 -1.325	1.386 -3.337	3.490 -9.530	9.484 3.701	6.130 0.541	-0.904 6.357
G 1000	X 0.060	-3.469 -1.239	1.357 -3.220	3.314 -9.229	8.991 3.532	5.300 0.195	-0.589 6.122
H 1000	X 0.060	-3.523 -1.317	1.349 -3.323	3.568 -10.351	10.329 3.932	6.991 0.485	-0.819 7.482
E 1000	Y 0.092	-2.900 -0.776	0.922 -2.714	3.269 -8.331	8.724 3.483	5.250 0.724	-0.763 5.745
A 1000	S 0.000	-0.620 -0.516	0.302 -0.213	1.685 -3.874	3.739 2.057	6.202 -0.161	-0.237 6.802

Rotordynamic Matrices

As mentioned earlier, rotordynamicists much prefer the [K]-[C]-[M] format. Dimensionless values of the elements of the [K], [C] and [M] matrices obtained from second order least squares fits to the elements of $[A(\Omega/\omega)]$ are presented in Table 1. It is clear from Figures 6 and 7 that the curvature of the graph of the average tangential force, F_T, is small and somewhat uncertain below the design flowrate. This results in appreciable departures from the pure quadratic behavior and, hence, discrepancies in the off-diagonal terms of some of the inertia matrices, [M]. On the other hand, the elements of the stiffness matrices, [K], are in good agreement with the measurements of Chamieh, et al. [3,4,5]. Selected values from Table 1 are used in the rotordynamic analysis of the SSME High Pressure Oxygen Turbopump (HPOTP). This analysis was carried out by Childs and Moyer and is appended herein.

SUMMARY AND CONCLUSIONS

Measurements of the complete hydrodynamic force matrices were presented for various impeller-volute/diffuser geometries and various pump operating conditions. The common assumption of skew-symmetry for these matrices is justified. Conventional scaling of forces with pump speed was perfectly demonstrated. The results obtained at and above design flow conditions closely support the commonly used quadratic variation with whirl frequency. As expected, the rotordynamic coefficients are very sensitive to the value of the flow coefficient, especially below design conditions. On the other hand, the presence, number, or orientation of diffuser guides have surprisingly little effect on the results.

As for the effect of the impeller geometry, a definite conclusion should not be made until impellers with more dissimilar characteristics are tested. To this end, the pump inlet section will be modified to accommodate the HPOTP inducer/impeller which will be tested in the near future. Also, leakage flow and preliminary cavitation tests are underway.

NOMENCLATURE

[A]	dimensionless hydrodynamic force marix
[C]	hydrodynamic damping matrix as defined by Equation (3)
b_2	impeller discharge width
{F}	6-component generalized force vector
F_1,F_2	components of instantaneous lateral force on impeller in the rotating balance reference frame
F_x,F_y	components of instantaneous lateral force on impeller in fixed laboratory reference frame (X,Y) non-dimensionalized by $\rho\pi r_2^3\omega^2 b_2$
F_{ox},F_{oy}	values of F_x and F_y when impeller axis remains coincident with the origin of the (X,Y) coordinate system
F_N,F_T	components of lateral force on impeller normal to and tangential to the whirl orbit, non-dimensionalized by $\rho\pi r_2^2\omega^2 b_2\epsilon$, averaged over one orbit
F_N,F_T	values of F_N,F_T averaged over one orbit
I,J	integers such that $\Omega = I\omega/J$
[K]	hydrodynamic stiffness matrix as defined by Equation (3)
[M]	hydrodynamic inertia matrix as defined by Equation (3)
N	pump rpm $= 60\omega/2\pi$
r_2	impeller discharge radius
t	time
(X,Y)	fixed laboratory reference frame
x,y	instantaneous coordinates of impeller center in fixed laboratory reference frame (X,Y), non-dimensionalized by r_2
$\dot{x},\dot{y},\ddot{x},\ddot{y}$	first and second time derivatives of impeller position, non-dimensionalized using the distance r_2 and the time ω^{-1}
ϵ	radius of circular whirl orbit
ρ	density of water
ϕ	pump flow coefficient based on impeller discharge area and tip speed
ψ	pump total head coefficient, total head rise divided by $\rho r_2^2\omega^2$
ω	radian frequency of pump shaft rotation
Ω	radian frequency of whirl motion $= I\omega/J$

APPENDIX A

IMPELLER NAME	OUTLET DIAMETR (mm)	OUTLET WIDTH (mm)	BLADE ANGLE (deg)	NUMBER BLADES	SPCFC SPEED	DESGN FLOW COEFF
X	161.9	15.8	23	5	0.57	0.092
Y	162.1	16.5	30	6		0.95
S	CONSOLIDATED DUMMY DUPLICATING OUTSIDE GEOMETRY OF IMPELLER X					

VOLUTE NAME	VOLUTE TYPE	CROSS SECTION SHAPE	SPIRAL ANGLE (deg)	TONGUE ANGLE (deg)	NUMBER VANES	VANE SECTOR (deg)
A	VOLUTE	TRAPE-ZOIDAL	4	174	0	NA
D (D-0)	VANELESS DIFFUSER	TRAPE-ZOIDAL	4	168	0	NA
E	VANED DIFFUSER	ELLIPTIC	5	140	17	26
F (D-F6)	VANED DIFFUSER	TRAPE-ZOIDAL	4	168	6	42
G (D-G6)	VANED DIFFUSER	TRAPE-ZOIDAL	4	168	6	33
H (D-H12)	VANED DIFFUSER	TRAPE-ZOIDAL	4	168	12	33

REMARKS:

1. Tongue angle = angle between upward vertical and line joining volute center to volute tongue.
2. F is Diffuser Volute D fitted with 6 long vanes. G is Diffuser Volute D fitted with 6 short vanes. H is Diffuser Volute D fitted with 12 short vanes. The longer vanes are fitted at a shallower angle.
3. The characteristics of Diffuser Volute E are close to those of the HPOTP. Volute E was made by Rocketdyne Division, Rockwell International.
4. Vane sector = angle subtended by vane.

APPENDIX A (cont.)

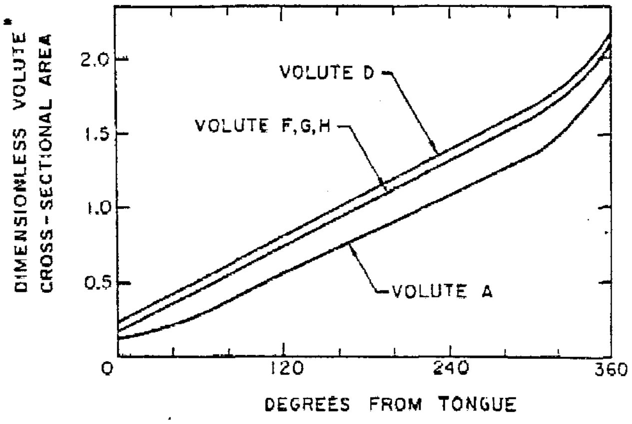

*DIMENSIONLESS AREA = AREA / $b_2 r_2$

REFERENCES

1. Ehrlc, F. and Childs, D., "Self-Excited Vibration in High-Performance Turbomachinery," Mechanical Engineering, *106*, (5), pp. 66-79 (May 1984).
2. Brennen, C. E., Acosta, A. J. and Caughey, T. K., "A Test Program to Measure Cross-Coupling Forces in Centrifugal Pumps and Compressors," Proceedings Workshop on Rotordynamic Instability Problems in High Performance Turbomachinery, Texas A&M University (May 1980), NASA Conference Publication 2238.
3. Chamieh, D. S., Acosta, A. J., Brennen, C. E., Caughey, T. K. and Franz, R., "Experimental Measurements of Hydrodynamic Stiffness Matrices for a Centrifugal Pump Impeller," Second Workshop on Rotordynamic Instability Problems in High Performance Turbomachinery, Texas A&M University (May 1982).
4. Chamieh, D. S., "Forces on a Whirling Centrifugal Pump—Theory and Experiments," Ph.D. Thesis, Division of Engineering and Applied Science, California Institute of Technology (February 1983).
5. Chamieh, D. S., Acosta, A. J., Brennen, C. E. and Caughey, T. K., "Experimental Measurements of Hydrodynamic Radial Forces and Stiffness Matrices for a Whirling Centrifugal Pump Impeller," (Submitted to J. Fl. Eng.).

6. Jery, B. and Franz, R., "Stiffness Matrices for the Rocketdyne Diffuser Volute," California Institute of Technology, Div. of Eng. and Appl. Sci., Report No. E429.1 (October 1982).
7. Jery, B., Acosta, A. J., Brennen, C. E., and Caughey, T. K., "Hydrodynamic Impeller Stiffness, Damping and Inertia in the Rotordynamics of Centrifugal Pumps," Third Workshop on Rotordynamic Instability Problems in High-Performance Turbomachinery, Texas A&M University (May 1984).
8. Ohashi, H. and Shoji, H., "Lateral Fluid Forces Acting on a Whirling Centrifugal Impeller in Vanelen and Vaned Diffuser," Third Workshop on Rotordynamic Instability Problems in High-Performance Turbomachinery, Texas A&M University (May 1984).
9. Domm, H. and Hergt, P., "Radial Forces on Impeller of Volute Casing Pumps," *Flow Research on Blading,* Dzung, L. S., ed., The Netherlands: Elsevier Publishing Co., pp. 305-321 (1970).
10. Agostinelli, A., Nobles, D. and Mockridge, C. R., "An Experimental Investigation of Radial Thrust in Centrifugal Pumps," Trans. ASME, J. of Eng. for Power, *82*, pp. 120-126 (April 1960).
11. Alford, J. S., "Protecting Turbomachinery from Self-Excited Rotor Whirl," J. of Eng. for Power, *87*, pp. 333-344 (October 1965).
12. Thompson, W. E., "Fluid Dynamic Excitation of Centrifugal Compressor Rotor Vibrations," J. Fluid Engineering, *100*, pp. 73-78 (March 1978).
13. Doyle, H. E., "Field Experiences with Rotordynamic Instability in High-Performance Turbomachinery," First Workshop on Rotordynamic Instability Problems in High-Performance Turbomachinery, Texas A&M University, NASA Conf. Pub. 2133, pp. 3-13 (1980).
14. Ek, M. C., "Solution of the Subsynchronous Whirl Problem in the High Pressure Hydrogen Turbomachinery of the Space Shuttle Main Engine," Paper No. 78-1002, AIAA/SAE 14th Joint Propulsion Conf., Las Vegas, Nevada (July 1978).

ACKNOWLEDGMENTS

The authors are indebted to the NASA George Marshall Space Flight Center, Huntsville, Alabama, for their continued sponsorship of this research under contract NAS8-33108. We are also most grateful for the help given by graduate students D. Adkins and R. Franz, undergraduate W. Goda and staff member D. Brennen. Belgacem Jery would also like to thank Byron-Jackson Pump Division, Borg-Warner Industrial Products, Inc., for financial support.

ADDENDUM

SAMPLE ROTORDYNAMIC CALCULATIONS USING CAL-TECH ROTORDYNAMIC COEFFICIENTS

by
Dara W. Childs
Director, Turbomachinery Laboratories
Department of Mechanical Engineering
Texas A&M University
College Station, Texas
and
David S. Moyer
Space Shuttle Systems Engineer
McDonell Douglas Technical Services Company
Houston, Texas

INTRODUCTION

Engineers may well be curious as to the influence of the impeller-diffuser forces on the rotordynamic characteristics of an actual piece of turbomachinery. As a partial answer to this point, some calculated results are presented for the HPOTP (High Pressure Oxygen Turbopump) of the SSME (Space Shuttle Main Engine). The rotating assembly for this unit is illustrated in Figure A-1. The high operating speed range of 20,900-30,380 rpm and the relatively high specific gravity of liquid oxygen (1.137) are obviously not typical of commercial equipment; however, the results do show the very significant influence of the impeller rotordynamic coefficient.

IMPELLER ROTORDYNAMIC MODEL

The Cal-Tech data presented in Table 1 defines the following constant-coefficient face-displacement model

$$-\begin{Bmatrix}F_X\\F_Y\end{Bmatrix} = \begin{bmatrix}K_{XX} & K_{XY}\\K_{YX} & K_{YY}\end{bmatrix}\begin{Bmatrix}X\\Y\end{Bmatrix} + \begin{bmatrix}C_{XX} & C_{XY}\\C_{YX} & C_{YY}\end{bmatrix}\begin{Bmatrix}\dot{X}\\\dot{Y}\end{Bmatrix} + \begin{bmatrix}M_{XX} & M_{XY}\\M_{YX} & M_{YY}\end{bmatrix}\begin{Bmatrix}\ddot{X}\\\ddot{Y}\end{Bmatrix} \qquad (A.1)$$

However, an inspection of the data in this table shows that the matrices are approximately symmetric; hence, for the results presented here, the following simplified model is used

$$-\begin{Bmatrix} F_X \\ F_Y \end{Bmatrix} = \begin{bmatrix} K & k \\ k & K \end{bmatrix} \begin{Bmatrix} X \\ Y \end{Bmatrix} + \begin{bmatrix} C & c \\ -c & C \end{bmatrix} \begin{Bmatrix} \dot{X} \\ \dot{Y} \end{Bmatrix} + \begin{bmatrix} M & m \\ -m & M \end{bmatrix} \begin{Bmatrix} \ddot{X} \\ \ddot{Y} \end{Bmatrix} \quad (A.2)$$

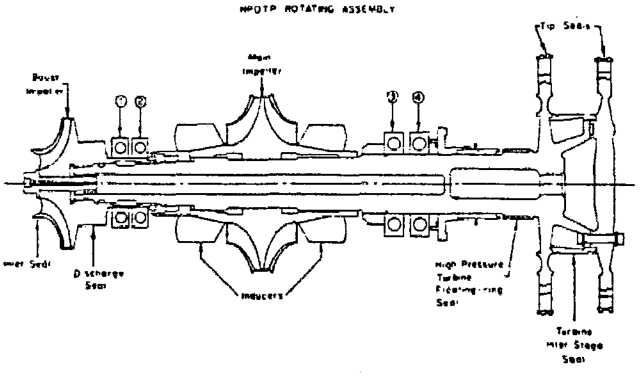

Figure A.1 HPOTP Rotating Assembly.

The dimensional entries of (A.2) are related to the nondimensional entries of Table 1 as follows

$$K = (K^*_{XX} + K^*_{YY})\ C_I\omega^2/2$$
$$k = (K^*_{XX} - K^*_{XY})\ C_I\omega^2/2$$
$$C = (C^*_{XX} + C^*_{YY})\ C_I\omega/2$$
$$c = (C^*_{XY} - C^*_{YX})\ C_I\omega/2$$
$$M = (M^*_{XX} + M^*_{YY})\ C_I/2$$
$$m = (M^*_{XY} - M^*_{YX})\ C_I/2$$

where * denotes the nondimensional entries of Table 1.
Further,

$C_I = \rho\pi b_2 \mu_2{}^2$

ρ = fluid density

r_2 = impeller discharge radius

b_2 = impeller discharge width.

For the main impeller of the HPOTP, $r_2 = 85$ mm, and $b_2 = 25.4$ mm, while for the boost impeller, $r_2 = 66$ mm, and $b_2 = 6.9$ mm. The fluid density for both impellers is approximately 1100 kg/m^3.

Most computer codes in use today for pump rotordynamics analysis do not account for the added-mass coefficients of Equation (A.2). The authors of this addendum extended the procedure of [A.1] to account for added mass terms in carrying out the calculations presented here.

ROTORDYNAMIC CALCULATIONS

Over the past several years, the HPOTP has experienced excessive subsynchronous motion at a frequency associated with a second critical speed mode shape. The zero-running-speed undamped modes are illustrated for the first and second rotor bending modes in Figure A-2. Observe that the first critical speed mode shape involved primarily the overhung turbine mode with relatively small bearing deflections, while the second mode involved large deflections at the main impeller and large bearing deflections. Hence, the first mode response is expected to be insensitive to impeller forces, while the second mode would be quite sensitive.

The addendum authors recently published the result of a rotordynamic analysis concerning subsynchronous vibration problems of the HPOTP [A-2] when operating at high speeds. The rotordynamics model used in [A-2] included a structural dynamics model for the rotor and the housing. For linear analysis, the bearings were modelled as linear springs. Liquid seals at the boost impeller were modelled according to Equation (A-2) using the analysis procedure of [A-3]. Gas seals in the turbine area were accounted for by a model similar to Equation (A-2), except that the mass matrix was dropped. Seal coefficients were calculated based on Nelson's analysis [A-4]. The turbine clearance excitation forces used the model of Thomas [A-5] and Alford [A-6].

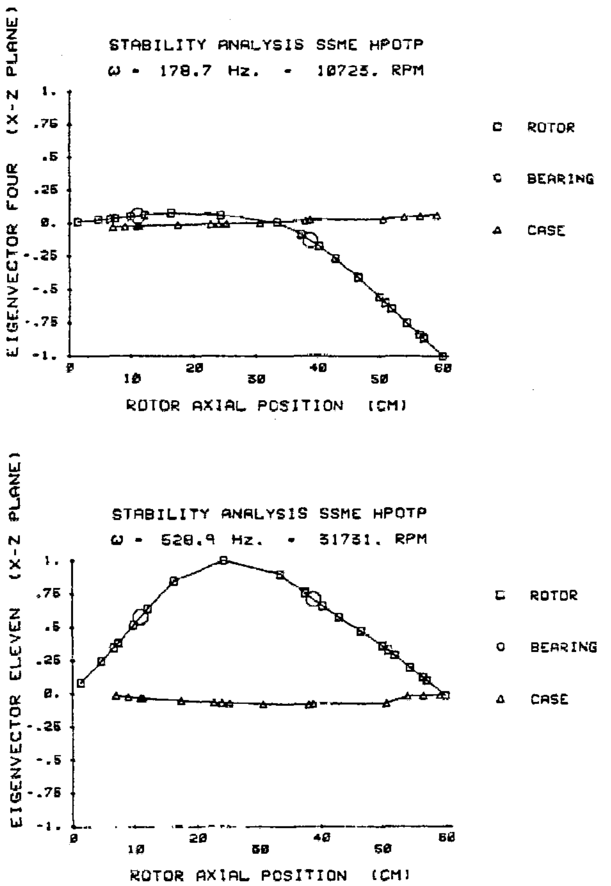

Figure A.2 Undamped, Zero-Running-Speed, Rotor-Housing Modes Associated with the First and Second Rotor Critical Speeds.

The obvious point of interest here is the influence that the impeller coefficients had on the rotordynamics characteristics of the HPOTP. This point is addressed by calculating the OSI (Onset Speed of Instability) and synchronous bearing reactions for the following impeller models:

- Stiffness Coefficients only. This was the first "static-only" data published by Chamieh, et al. [3] and was used in [A-2].
- Full model, including stiffness, damping, and added-mass coefficients.
- Reduced model, obtained by dropping the added-mass terms.
- Reduced model, obtained by dropping the added-mass terms and the cross-coupled damping terms.

The nondimensional data for Volute A, $\phi = 0.092$ of row 4 in Table 1 are used.

The synchronous reactions for bearings 1 and 4 due to rotating imbalance based on only the stiffness-matrix model for the impellers are illustrated in Figure A-3. The bearing-reaction response was dominated by first and second critical speeds at approximately 13,500 rpm and 31,170 rpm, respectively. Some smaller peaks are evident, due to housing resonances. The calculated OSI for this configuration was approximately 30,500 rpm. The cross-coupled stiffness coefficient from the main impeller was the source of the instability, and the OSI was arbitrarily set to the calculated value by adding direct damping at the main impeller. The OSI of 30,500 rpm was chosen to yield agreement with field data.

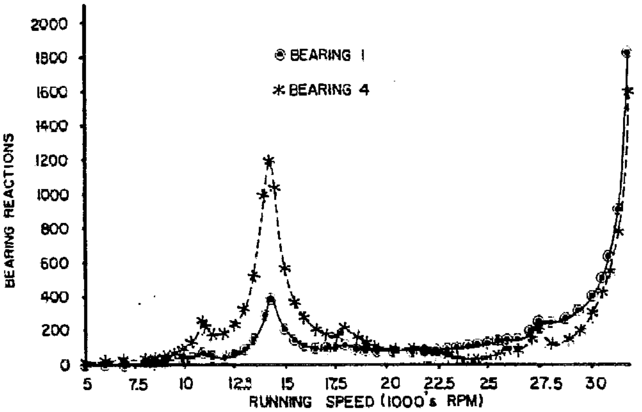

Figure A.3 Calculated Bearing Reactions for Stiffness-Matrix-Only Impeller Models.

The results presented in Figure A-4 illustrate the predicted synchronous-response characteristics including the stiffness, damping, *and* added mass terms. The second critical speed was calculated to lie at 33,060 rpm, while the predicted OSI was greater than 55,000 rpm.

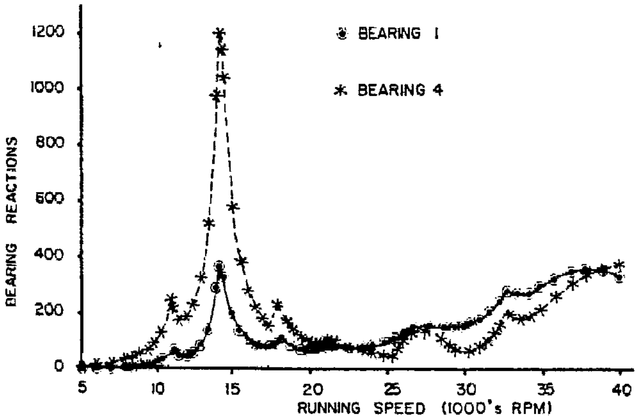

Figure A.4 Calculated Bearing Reactions for Full Impeller Models Including Stiffness, Damping, and Added-Mass Matrices.

The results presented in Figure A-5 illustrate the calculated bearing reactions if the stiffness and damping matrices are included, but the mass matrix is dropped. The second critical speed is seen to be heavily damped and was elevated to approximately 39,000 rpm. For this impeller model, the OSI was also greater than 55,000 rpm. By comparison with Figure A-4, the obvious conclusion is that the mass-matrix contribution can not be neglected, and rotordynamics-analysis procedures for pumps, which are not able to account for the added-mass matrix at impellers, should be avoided.

The cross-coupled-damping coefficients in the models of equations (A-1) and (A-2) act as "gyroscopic-stiffening" elements to raise the rotor's critical speed, and the Cal-Tech cross-coupled damping coefficients are relatively high. The direct mass coefficients tend to compensate for the cross-coupled damping coefficients in depressing the rotor critical speeds, and this explains the sharp elevation of the second critical speed from Figure A-4 to Figure A-5 after the mass matrix has been dropped. From this reasoning, one could expect that dropping both the mass matrix *and* the cross-coupled damping matrix might yield a simplified, but still reasonable, model. The synchronous response prediction for this type of impeller model is illustrated in Figure A-6. The second critical speed is predicted to be at 32,340 cpm, which is in reasonable agreement with the results of Figure A-6 for the complete impeller model; however, the second critical speed is much more heavily damped and the predicted OSI is now in excess of 75,00 cpm. Clearly, the proposed simplified model is inadequate.

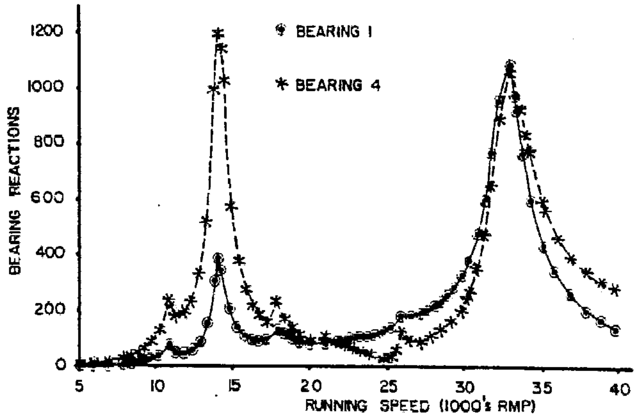

Figure A.5 Calculated Bearing Reactions for Reduced Impeller Models with the Mass Matrix Dropped.

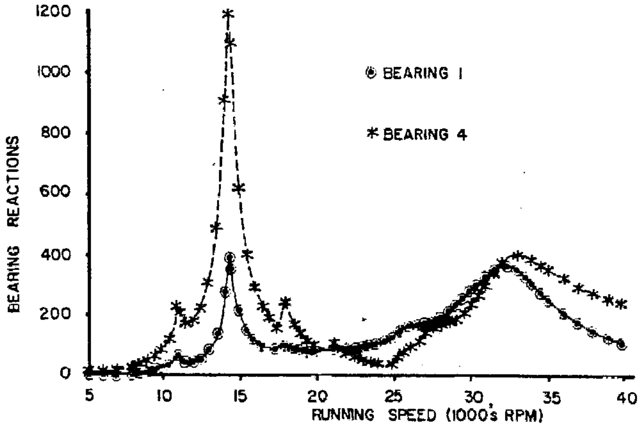

Figure A.6 Calculated Bearing Reactions for a Reduced Impeller Model Including the Stiffness Matrix and the Direct-Damping Coefficients.

CONCLUSIONS

The sample calculations presented herein support the following conclusions:

(a) Impeller-diffuser forces have a very significant impact on the calculated rotordynamic characteristics of pumps, particularly with respect to damping and stability

(b) The complete model for the impeller, *specifically including the mass terms*, must be included in rotordynamic calculations to achieve reasonable results.

REFERENCES

A.1 Childs, D. W., "The Space Shuttle Main Engine High-Pressure Fuel Turbopump Rotordynamic Instability Problem," Trans. ASME, Journal of Engineering for Power, *100*, pp. 48-57 (January 1978).

A.2 Childs, D. W. and Moyer, D. S., "Vibration Characteristics of the HPOTP of the SSME," ASME Gas Turbine Conference, Paper 84-GT-31, Amsterdam, The Netherlands (June 1984).

A.3 Childs, D. W., "Finite-Length Solutions for Rotordynamic Coefficient of Turbulent Annular Seals," Trans. ASME, Journal of Lubrication Technology, *105*, pp. 437-445 (July 1983).

A.4 Nelson, C. D., "The Rotordynamic Coefficients of High-Pressure Annular Gas Seals," ASME Gas Turbine Conference Paper 84-GT-32, Amsterdam, The Netherlands (June 1984).

A.5 Thomas, J. J., "Instabilie Eigenschwingungen von Turbine Laufern, angefacht durch die Spalstromungen Stopfbushsen un Beschaufelungen," *AEG-Sonderdruch* (1958).

A.6 Alford, J., "Protecting Turbomachinery from Self-Excited Rotor Whirl," Trans. ASME, Journal of Engineering for Power, pp. 333-343 (October 1965).

ACKNOWLEDGMENT

This work was supported in part by NASA Contract NAS8-34505, from the George C. Marshall Space Flight Center.